GA–A23948

APPROACH TO STEADY-STATE DISCHARGES ON DIII–D

by

R. PRATER, A.M. GARAFALO, R.W. HARVEY, D.A. HUMPHREYS,
R.J. LA HAYE, T.C. LUCE, M. MURAKAMI, F.W. PERKINS,
P.I. PETERSEN, C.C. PETTY, P.A. POLITZER, E.J. STRAIT,
M.R. WADE, AND THE DIII–D TEAM

APRIL 2002

GA–A23948

APPROACH TO STEADY-STATE DISCHARGES ON DIII–D

by

R. PRATER, A.M. GARAFALO,[1] R.W. HARVEY,[2] D.A. HUMPHREYS, R.J. LA HAYE, T.C. LUCE, M. MURAKAMI,[3] F.W. PERKINS,[4] P.I. PETERSEN, C.C. PETTY, P.A. POLITZER, E.J. STRAIT, M.R. WADE,[3] AND THE DIII–D TEAM

This is a preprint of an invited paper presented at the Third IAEA Technical Committee Meeting on Steady-State Operation of Magnetic Fusion Devices, May 2–3, 2002, Arles, France, and published in the *Proceedings* (on CD-ROM only).

Work supported by U.S. Department of Energy under Contracts DE-FG03-99ER54463, DE-AC05-00OR22725, and DE-AC02-76CH03073, and Grants DE-FG02-89ER54461 and DE-FG03-99ER54541

[1]Columbia University
[2]CompX
[3]Oak Ridge National Laboratory
[4]Princeton Plasma Physics Laboratory

GENERAL ATOMICS PROJECT 30033
APRIL 2002

Approach to steady-state discharges on DIII–D

R. Prater, A.M. Garofalo,[1] R.W. Harvey,[2] D.A. Humphreys, R.J. La Haye, T.C. Luce, M. Murakami,[3] F.W. Perkins,[4] P.I. Petersen, C.C. Petty, P.A. Politzer, E.J. Strait, M.R. Wade,[3] and the DIII–D Team

General Atomics, P.O. Box 85608, San Diego, California 92186-5608

Abstract. The approach of the DIII-D program to steady-state operation is to improve the normalized performance so that the same real performance can be attained at reduced plasma current. The reduction in plasma current increases the fraction of the plasma current generated by the bootstrap effect, thereby reducing the requirements on the efficiency of the current drive systems. The current drive systems are still needed in order to support the remaining current and to sustain the profiles which give rise to the improvement in normalized performance. In DIII-D electron cyclotron current drive is used for this purpose. Recent experiments have validated the codes used to predict ECCD. At the higher normalized beta, MHD modes like the neoclassical tearing mode and the resistive wall mode become serious limitations on performance. The NTM may be stabilized using localized ECCD while the RWM can be suppressed through improved symmetrization of the confining magnetic fields. Discharges with full noninductive current and high bootstrap fraction have shown the need to address the long term evolution of such discharges.

Introduction

A tokamak operating economically in steady-state with high performance can only be achieved by making use of the Advanced Tokamak (AT) approach [1]. It is well known that the power efficiency of known current drive techniques is too low to drive a large fraction of the plasma current without making the overall power gain too small for economic viability. A way around this is to make use of the bootstrap current, which is self-generated by the radial gradients in density and temperature. If the bootstrap fraction can be made larger than 0.7, then the efficiency of the current drive for the remaining current is much less of an issue.

For steady state operation the bootstrap fraction must be large, but high fusion performance is also required. High performance requires high β (= plasma pressure/magnetic pressure) for high reactivity, which is proportional to β^2. The difficulty is that high fusion gain and high bootstrap fraction place conflicting requirements on the plasma current. Both theory and experiments show that for a given geometry, pressure profile, and toroidal field, the β is proportional to I_p, the plasma current. Hence, the fusion reactivity is proportional to I_p^2. On the other hand, the bootstrap fraction is proportional to β_p, the beta poloidal, which is inversely

[1]Columbia University, New York, New York
[2]CompX, Del Mar, California
[3]Oak Ridge National Laboratory, Oak Ridge, Tennessee
[4]Princeton Plasma Physics Laboratory, Princeton, New Jersey

proportional to I_p. So high bootstrap fraction requires low current while high performance requires high current. The β limit is written in terms of $\beta_N = (I_{MA} / B_T a_m)$, the normalized beta, since this quantity is a key parameter in the theory of stability limits. Since $\beta\beta_p$ is proportional to β_N^2, very high β_N is required if both β and β_p are to be high

A third major issue affected by the plasma current is disruptions. If a plasma disruption occurs in which the plasma current is lost on a short time scale, the release of the energy stored in the poloidal magnetic field results in extremely large forces and other stresses on the vacuum vessel structure and its interior parts and the coils. These forces may be destructive in the worst cases. But the magnetic energy stored in the poloidal field is proportional to I_p^2, while $j \times B_T$ forces are proportional to I_p. So reduction of the plasma current also will mitigate the impact of disruptions.

The AT program addresses these issues by seeking to increase confinement and stability through control of the plasma shape, the radial profile of plasma current, the plasma rotation profile, and MHD instabilities. Noting the definitions $\beta_N = \beta / (I_p / aB_T)$ and $H = \tau_E / \tau_{E,ITER89P}$ where $\tau_{E,ITER89P}$ is the energy confinement scaling developed from a fit to a broad experimental data base, the concept is to increase both β_N and H through operation of a tokamak with optimized shape and profiles. In that way the same fusion gain can be obtained at lower current, while the lower current makes high bootstrap fraction possible and reduces the potential impact of disruptions. It should be noted that high normalized performance— characterized as large $\beta_N H$ — does not imply an increase in real performance; rather, the vision is of similar real performance at smaller but potentially steady-state plasma current.

The Advanced Tokamak Approach

In a conventional tokamak, the plasma current is supported through an electric field applied inductively. The resultant current profile is peaked at the center where the electrical conductivity is highest. This usually results in the central safety factor, q, lying slightly below unity, which leads to the strong MHD sawtooth instability. One approach to the AT is to make the current profile very broad or even hollow [1,2]. This has a number of beneficial effects. The minimum of the safety factor, q_{min}, can be made to rise above low order rational numbers, typically 1, 3/2, 2, and possibly even 5/2, thereby completely eliminating some of the strong low-order internal MHD instabilities. The magnetic shear which results from the optimized current profile is negative, which permits high pressure gradients in the plasma core. These high pressure gradients generate a large bootstrap current in their vicinity, hence the bootstrap current is driven strongly at the off-axis location needed to support the hollow current profile. Finally, the external MHD modes are pushed outside the off-axis current peak, relatively closer to the outer edge of the plasma where the stabilizing influence of the electrically conducting vacuum vessel is improved. A model example of the current and safety factor profiles is shown in Fig. 1 for this Negative Central Shear (NCS) concept.

The DIII-D AT program aims to realize such discharges. The approach to generating the optimized current profile is to apply plasma heating early in the discharge while the plasma current is increasing. The heating increases the conductivity, slowing the rate at which the current penetrates to the core, thereby generating a NCS current profile, at least transiently. As

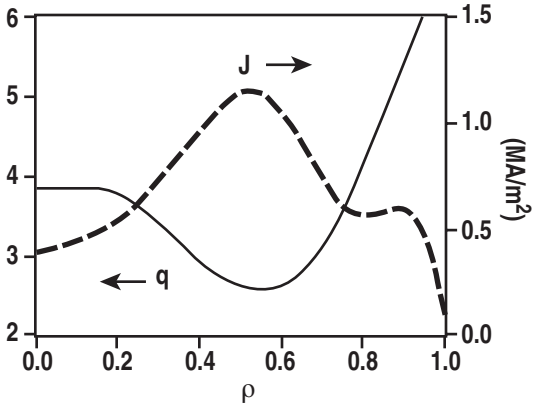

Fig. 1. Model hollow current and q profile for an AT discharge.

an example Fig. 2 shows two discharges, an AT discharge with neutral beam heating applied very early in the discharge and a conventional discharge for comparison [3]. High power NBI is applied to both discharges after a steady current is reached. Figure 2 shows that higher β_N and H are attained in the AT discharge, so that the β and τ_E are about the same for the two discharges even though the plasma current is 40% smaller in the AT case. Importantly, the bootstrap fraction $f_{bootstrap}$ is nearly three times higher in the AT discharge, reaching

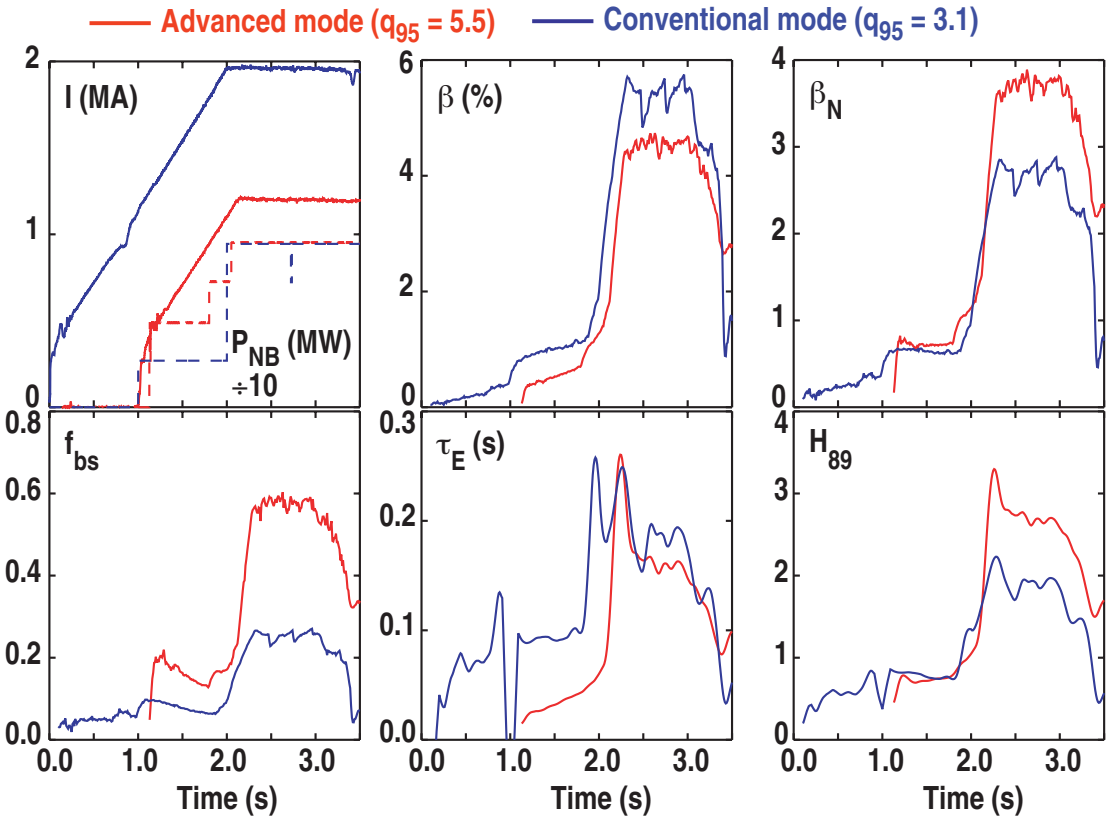

Fig. 2. A conventional discharge (blue; $q_{95} = 3.1$) and an AT discharge (red; $q_{95} = 5.5$) from DIII–D. Shown are the plasma current, the total β, the normalized beta, the bootstrap fraction, the energy confinement time, and the confinement factor relative to the ITER-89P empirical scaling.

0.6. Still larger $f_{bootstrap}$ is ultimately required. The AT discharge of Fig. 2 lasts about 0.7 s, limited by MHD instabilities (a resistive wall mode coupled to a $m = 1 / n = 1$ tearing mode).

Discharges with high normalized performance which are stationary on the time scales of the energy confinement and current profile relaxation have been attained in DIII–D [4]. A key technology development in achieving this performance is the feedback control of the heating power to keep the plasma β at a preprogrammed value. Without this feedback the increase in confinement characteristic of the AT mode was found to cause the stability limits to be reached, resulting in sudden loss of performance. A discharge using such feedback is shown in Fig. 3. Here, the β is maintained at 90% of the $m = 1 / n = 1$ tearing mode limit (where m and n are the toroidal and poloidal mode numbers, respectively), and the high performance of $\beta_N H \sim 7$ was obtained for a period of $34\tau_E$, or several times the resistive time scale. (However, the bootstrap fraction is only about 0.35.) Internal measurements of the magnetic field show that the current profile is in fact in a stationary state, although a small inductive voltage is needed to maintain the current. The particle balance indicates that the wall is in equilibrium (neither a net source nor sink of particles) and the impurity concentration is not increasing

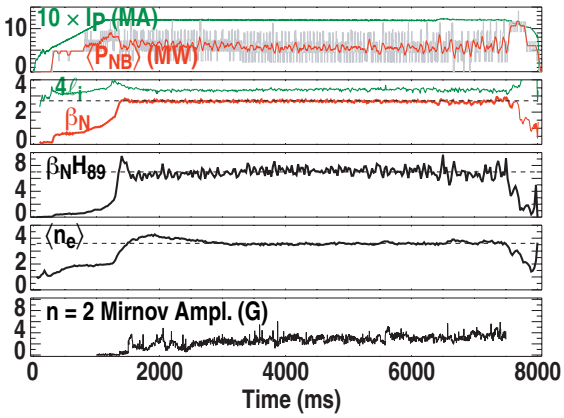

Fig. 3. Traces from a stationary discharge with high normalized performance. The plasma β is controlled to a fixed level through feedback to the NBI heating. The first box shows both the actual power and the time averaged power.

The progress in attaining long discharges at high performance is shown in Fig. 4. The program objective is shown as $\beta_N H$ in the range 10 to 15 for durations of 10 to 30 times the energy confinement time. Discharges in H–mode with edge localized modes (ELMs) and with q_{min} above 1.5 and stationary pressure profiles have been most successful in approaching the target range. It is essential to note that high absolute performance is sought as well as high normalized performance, and many of the discharges of Fig. 4 exceed the β target of ITER. The discharge of Fig. 2, for example, has volume-averaged β exceeding 4%.

The duration of the discharges of Fig. 4 is limited in many cases by a slow evolution of the current profile. Extensive modeling [5] has been performed to determine how this evolution may be avoided through use of the rf heating systems available or planned for DIII–D. The general approach is to start with an experimental discharge which exhibits high performance and add localized current drive power to sustain the current profile. The transport coefficients are determined from the experimental result, but they are scaled with increases in the power to be consistent with the global power dependence of confinement. This approach is used to obtain maximum credibility for the results, as the final state is not far from the initial state. The modeling uses the TORAY-GA ray tracing code to study the effects of electron cyclotron heating (ECH) and current drive (ECCD), using the parameters characterizing the ECH system (e.g., the ray launching angles, dispersion, and locations) as implemented on DIII–D. The ECH system operates at 110 GHz and uses low-field-side launch of the second harmonic extraordinary mode. The ECH power is generated by six gyrotrons with coupled power in the range of 0.5 to 0.8 MW each, and in this study we use 3.5 MW as the total coupled power.

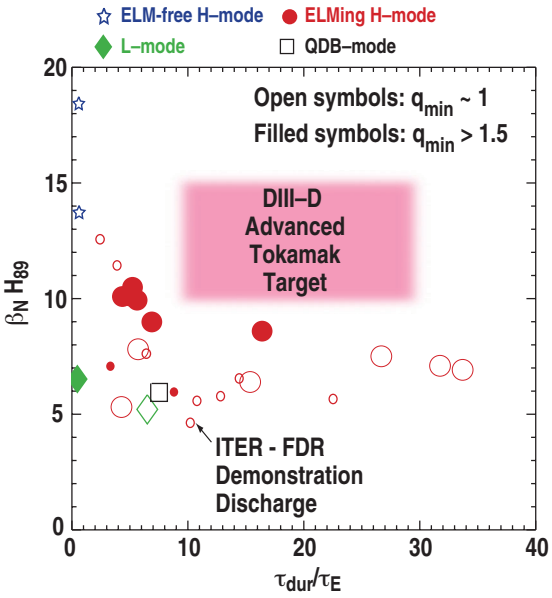

Fig. 4. Plasma performance in DIII–D, as measured by $\beta_N H_{89}$, versus the duration of the high performance phase normalized by the energy confinement time. Shown are ELM-free H–mode discharges (star), ELMing H–mode discharges (circles), and L–mode discharges (diamonds).

The modeling predicts that the current driven by the ECH power, if properly distributed radially, can sustain a discharge with $\beta_N = 4$ and $H_{89P} = 3.1$ with $f_{bootstrap} = 0.65$ for more than the 10 s duration of the toroidal field system on DIII–D. The evolution of the safety factor is shown in Fig. 5(a) and the components of the current in the final state are shown in Fig. 5(b). The initial state (derived from experiment) is shown as the dotted lines in Fig. 5. The changes in the ion and electron temperature profiles are modest, as shown in Fig. 5(c), indicating that the changes from the initial state of the calculated neutral beam current drive and bootstrap current are not large. A key approach is to spread the ECCD adequately in space, as illustrated by the j_{EC} curve in Fig. 5(b) The j_{EC} generated by a single ECCD system is much narrower than the peak of this curve, but by aiming the ECH systems slightly differently the net current drive can be spread, resulting in much better agreement of the final net current profile with the initial profile. This work implies that steady-state discharges with $\beta_N H_{89P} = 12$ and adequately high $f_{bootstrap} = 0.65$ can be attained in DIII–D in the near term.

Sustainment of current profile by ECCD

The efficiency of ECCD has been extensively studied in DIII–D in order to validate the physics models on which the calculations are based [6]. The physics model is embodied in the TORAY-GA code, which uses ray tracing to determine the wave absorption and the model by Cohen [7] for current drive, and in the CQL3D Fokker-Planck code [8]. The absorption calculated by TORAY-GA has been validated in detail through application of modulated ECH and phase sensitive detection of the perturbed electron temperature [9], but until recently the comparison with the current drive model has been incomplete. Development of a technique to compare the magnetic field pitch angles determined from the motional Stark effect (MSE) diagnostic with simulated pitch angles calculated from the equilibrium (a "synthetic diagnostic") [10] has provided a way to determine the profile of driven current with a radial resolution equal to that of the spacing between MSE channels. Alternatively, the driven current can be derived from evolution in time and space of the flux in the plasma, under the assumption of neoclassical electrical resistivity [11]. Under the conditions of many experiments on DIII–D, the toroidal electric field is not negligible. (The profile of the toroidal electric field can be determined from the time behavior of the MSE signals.) In these cases and to include the effects of distortions of

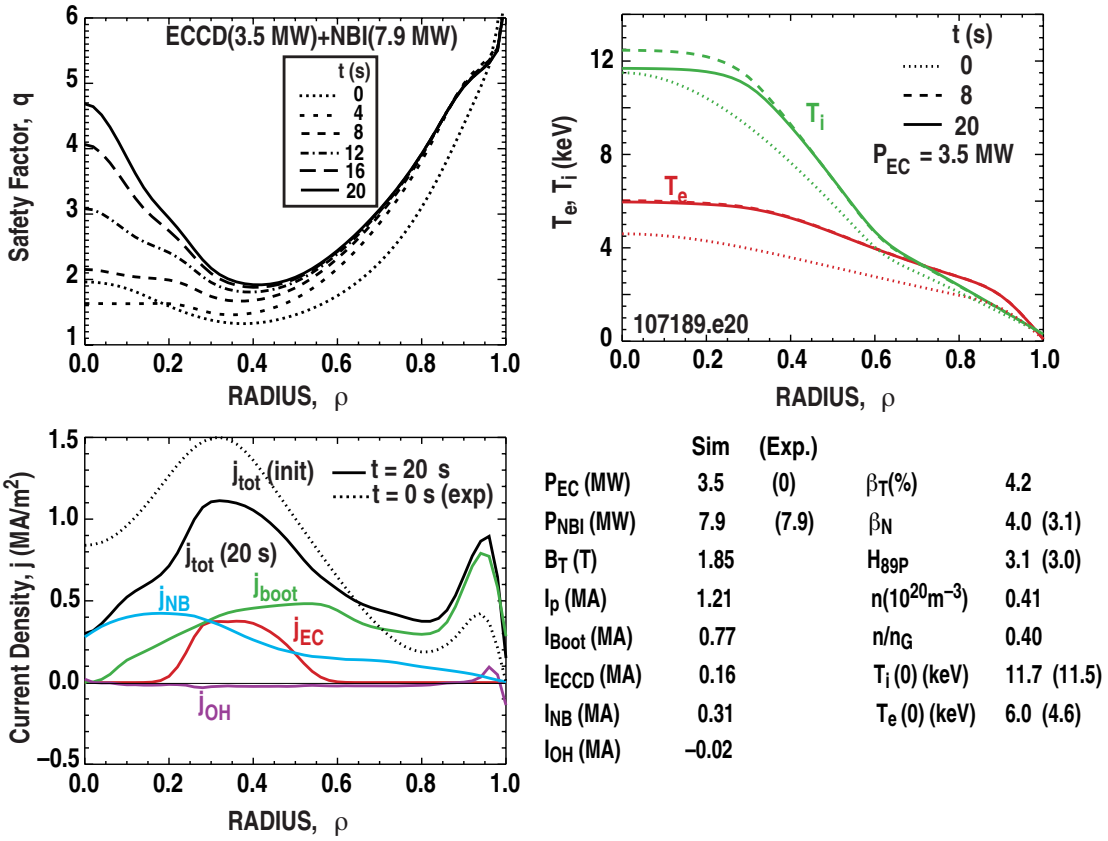

	Sim	(Exp.)		
P_{EC} (MW)	3.5	(0)	β_T(%)	4.2
P_{NBI} (MW)	7.9	(7.9)	β_N	4.0 (3.1)
B_T (T)	1.85		H_{89P}	3.1 (3.0)
I_p (MA)	1.21		$n(10^{20}m^{-3})$	0.41
I_{Boot} (MA)	0.77		n/n_G	0.40
I_{ECCD} (MA)	0.16		T_i (0) (keV)	11.7 (11.5)
I_{NB} (MA)	0.31		T_e (0) (keV)	6.0 (4.6)
I_{OH} (MA)	–0.02			

Fig. 5. Profiles developed from modeling using the ONETWO transport code. In all cases the dotted lines represent the initial profiles and the solid lines represent the profiles following 20 s of evolution.

the electron distribution function from a Maxwellian the Fokker-Planck code must be used for calculating the driven current. This code includes the self-consistent effects of the electric field, as well as a more physically accurate model for the collision operator and conservation of momentum in electron-electron collisions. Application of these quantitative analysis techniques has provided an accurate picture of the ECCD profile in DIII–D under a broad range of conditions.

The Fokker-Planck code has proven to be an accurate predictor of current drive. Figure 6 shows the measured magnitude of driven current versus the current calculated from CQL3D [9]. The conditions of the experiment include a wide range of densities and temperatures and edge conditions (L–mode and H-–mode) and ray launch angles. The experiments also include a range of normalized minor radius ρ of up to 0.4. Clearly, the code is highly predictive of the magnitude of the current.

The agreement of the calculated ECCD with measured ECCD is particularly significant in regard to the dependence on the minor radius of the location of the current drive. As the minor radius increases, the fraction of electrons trapped in the magnetic well increases. This causes two effects. First, the ECCD generated by the Fisch-Boozer effect [12] decreases because a fraction of the ECH power is wasted on heating electrons which are trapped and therefore do

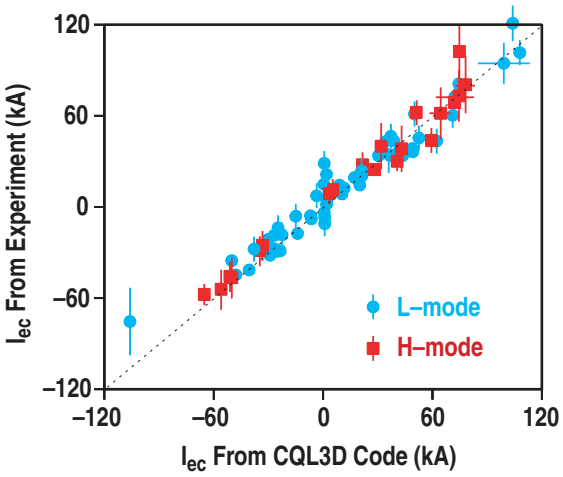

Fig. 6. The measured current driven by ECCD versus the current calculated by the CQL3D Fokker-Planck code for the experimental conditions. The dotted line represents perfect agreement. In all cases, the effects of the remaining dc electric fields are included in the calculations.

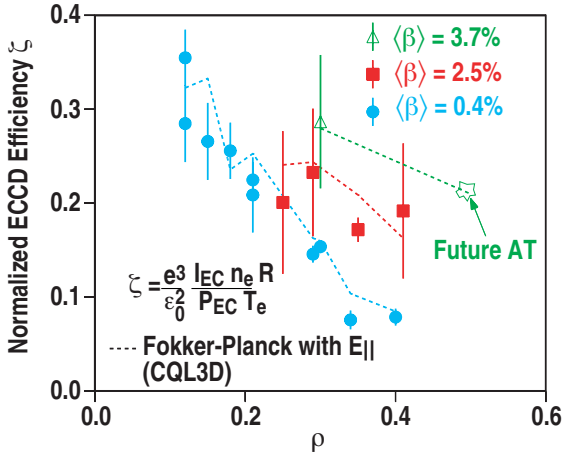

Fig. 7. Measured dimensionless current drive efficiency versus the minor radius where the peak current drive is taking place, for three values of average β. For each scan the $n_{||}$ is held roughly constant, and the current drive takes place along a vertical line running through the plasma center. The point labeled "Future AT" is taken from modeling like that of Fig. 5.

not contribute to the current drive. Second, Ohkawa has shown [13] that the asymmetric trapping and symmetric detrapping generates a current in the direction opposite the Fisch-Boozer current. The canceling effects may cause the off-axis current drive efficiency to approach zero under some conditions, which is certainly an issue for the Advanced Tokamak which requires off-axis current sustainment. However, recent experiments have shown that in higher performance plasmas a large increase in off-axis ECCD efficiency takes place, in agreement with the modeling calculations described above.

The improvement in off-axis ECCD efficiency with β is shown in Fig. 7 [9]. Here, the normalized dimensionless efficiency $\zeta = (e^3 / \varepsilon_0^2) I_{ECCD} n_e R / P_{ECCD} T_e$ is the current drive efficiency I_{ECCD} / P_{ECCD} normalized by the expected dependencies on density and temperature. The normalization removes the radial dependence of the density and temperature profiles, leaving the physical effects of the trapping. At the lowest $\langle\beta\rangle$ of 0.4%, the fall-off of efficiency with ρ is very strong due to the canceling effects discussed above. For higher β discharges which are more consistent with the AT modeling cases, the fall-off is much less significant and much of the reduction at lower β is recovered. For the modeled AT discharge similar to that of Fig. 5 the projected ECCD efficiency shown in Fig. 7 at $\rho = 0.5$ is only a small extrapolation from the measured cases, so confidence is high that the calculations accurately predict the future behavior.

The physics involved in the increase in the off-axis efficiency with β can be understood from the details of the modeling [14]. First, the imaginary part of the EC wavevector (the dissipative part) increases with density and temperature for the second harmonic extraordinary mode which is used in the experiments. The stronger absorption results in

deposition further from the cold plasma resonance, and hence on electrons with larger $v_{||}$ due to the Doppler shift. This larger $v_{||}$ means that the wave-particle interaction will be shifted further from the trapping region. At the same time, the larger electron temperature means that relativistic effects will be stronger, and one such effect is to cause the resonance in velocity space to curve away from the trapping boundary. Both effects reduce the flux of particles across the trapped electron boundary in velocity space. In order to see the total effect it is necessary to examine the contours of the total flux, which includes both the EC driven flux and the collisional flux that results in a steady-state distribution function. These fluxes are calculated by CQL3D, and they show how the collisional relaxation produces some increase in the flux into the trapped region even when the rf interaction is far from the trapping boundary [14]. Hence, there is some reduction in efficiency with ρ but the reduction is much smaller at higher β. All these effects are included in the modeling.

Control of MHD Modes

The AT operates at high bootstrap fraction obtained by operation at higher β_N, which can introduce MHD instabilities. Two such modes are the neoclassical tearing mode (NTM) and the resistive wall mode (RWM). On DIII–D the NTM has been stabilized under some conditions through application of highly localized ECCD [15], and the RWM has been controlled through optimized reduction of error magnetic fields [16].

The NTM is a tearing mode which may arise at high β even when the usual "classical" tearing mode is stable [17]. The physical concept is that if a helical magnetic island exists in the plasma, then the radial pressure gradient in the island will be small, so there will be a helically localized reduction in the bootstrap current. If the island is of sufficient size (larger than a threshold size), the helical current perturbation will cause the island to grow to a larger saturated state causing significant loss in plasma confinement. However, driving a localized current, for example by ECCD, within the island can replace the "missing" bootstrap current and stabilize the mode [18,19]. This process has been demonstrated for the $m = 3 / n = 2$ mode on several tokamaks using ECCD [20–22].

Results from DIII–D have shown that when the 3/2 mode is stabilized, the plasma pressure can be increased [15]. Figure 8 shows such a discharge. High power neutral beam heating is applied and the plasma β_N rises to 2.5. At that time, however, a 3/2 mode develops and grows to a saturated size. The transport caused by this island causes β_N to decrease to around 1.9, a drop of 25%. At 3000 ms the ECCD is applied at the predetermined radial location of the magnetic island. The ECCD causes the $n = 2$ mode amplitude to gradually vanish, and when additional neutral beam heating is applied the plasma β_N rises to new limit near 3.0, an increase to 20% above the initial limit on β_N and to 60% above the limit when the saturated island was present. Since the fusion performance is proportional to β_N^2, these increases are very significant.

In the discharge of Fig. 8, the sawtooth instability acts as the trigger which generates a magnetic island of sufficient size that mode growth takes place. The sawtooth can be seen as the periodic behavior of the $n = 1$ mode amplitude in Fig. 8(b). The sawteeth continue throughout this discharge, but after 3300 ms large "fishbone instabilities" are also present. The fishbone instability is caused by the presence of fast ions from the neutral beam, so it appears that decreasing

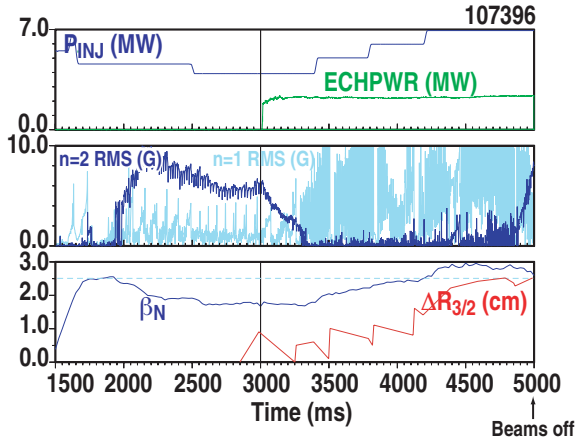

Fig. 8. Traces from a discharge in which ECH power is applied near the $q = 3/2$ surface to suppress the neoclassical tearing mode. (top) neutral beam and ECH power; (mid) $n = 2$ component of the fluctuating magnetic field due to the 3/2 NTM (dark blue), $n = 1$ component due to fishbone instabilities (light blue); (bottom) normalized beta (blue), relative location of the $q = 3/2$ surface (red).

the 3/2 magnetic island size improves the confinement of fast ions to the level where fishbone instabilities become large.

As the plasma pressure rises with increasing β_N, the major radius of the plasma increases (the "Shafranov shift"). This shift of the plasma location causes the ECCD to no longer be applied in the optimum location, and following the large sawtooth at 4850 ms in Fig. 8. the NTM grows again. This illustrates the need to have a system which can track the optimum location for the ECCD even when the mode is not present. Such a system is being implemented on DIII–D, using real-time calculations of the evolution of the $q = 3/2$ surface location for feedback purposes. The feedback can act on the toroidal field magnitude, on the plasma vertical or horizontal location, or ultimately on the launch angles of the ECH system to keep the ECCD in the correct location. This system can be combined with the robust "search and suppress" system which is now successfully in use to optimize the current drive location when the mode is large enough to be detected by the diagnostic [15].

In addition to the 3/2 NTM, it may also be necessary to stabilize the 2/1 NTM, which is more rapidly growing and which may result in a disruption. Efforts to stabilize the 2/1 mode have not been fully successful with ECH power at the 2.2 MW level, and extrapolation from the results indicates that ECH power near 3 MW may be needed. This will be tested in experiments shortly. However, it should be noted that the presence of low order rational surfaces like $q = 3/2$ and $q = 2$ is not consistent with the high $f_{bootstrap}$ goal of the AT program. Rather, these experiments are aimed at validating the physics and establishing the techniques for stabilization of higher order modes. Stabilization of the low order NTM may also be very useful for conventional pulsed tokamak devices which have a low value of the safety factor.

The resistive wall mode which can limit the duration of the high β phase of the discharge has also been addressed, by decreasing the error magnetic fields and by maintaining sufficient rotation drive [16]. MHD modes like the $n = 1$ kink mode which extend toward the boundary of the plasma can be stabilized by the image currents which flow in the conducting vacuum vessel wall. For the geometry of the DIII–D system the β_N can be made stable up to double (depending on the profiles) the calculated limit in the absence of a conducting wall. However, because the vacuum vessel is resistive, the image currents decay and wall stabilization becomes ineffective. Rotation of the plasma in combination with dissipation can maintain the stabilizing effect, but rotation slows as β_N exceeds the no-wall limit. If the rotation drops below a critical value, the resistive wall mode grows and the high β_N performance is lost.

The physical mechanism seems to be that above the no-wall limit an RWM which is stabilized by plasma rotation can still enhance the plasma response to the $n = 1$ error magnetic field present in the system. This causes the reduction in plasma rotation and subsequent destabilization of the RWM. The error magnetic field can be reduced by applying currents in a set of six evenly spaced coils mounted outside the vacuum vessel, at the outboard midplane. These coil currents can be controlled by feedback on the RWM amplitude at the vessel wall. Dynamic error correction by feedback control of the correction coil currents is used to optimize the magnetic environment and therefore the rotation. In the best cases, the β_N can be raised to 100% above the no-wall limit for extensive periods, as shown in Fig. 9. Calculations with the VALEN code [23] indicate that with a more optimized set of coils wound on the vacuum vessel, with six above the midplane and six below, the beta limit for an ideal wall (with no resistivity) can be reached even without plasma rotation. Such a coil set will be installed on DIII–D in summer, 2002.

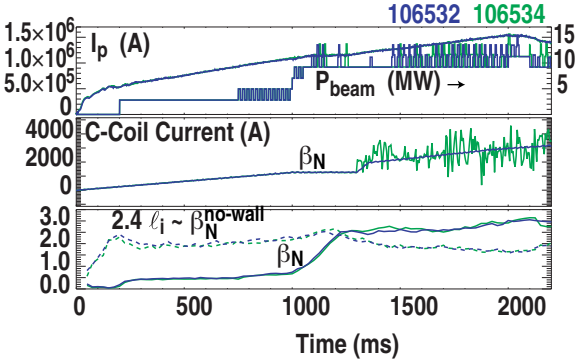

Fig. 9. Traces from a discharge with optimized error field reduction. (top) plasma current and neutral beam power; (mid) correction coil current; (bottom) 2.4 times the internal inductance (the calculated limit on normalized beta in the case of no conducting wall), and the β_N attained by the plasma. The green curves are for correction coil currents set using feedback on the magnetic perturations, and the black curves are for preprogrammed correction coil currents matching the average of the feedback case.

High Bootstrap Fraction

High confinement, high stability, and high bootstrap fraction are the three fundamental elements of the AT program. In the case of high bootstrap fraction, the bootstrap current which forms the majority of the total current has a radial profile which is determined by the gradients in density and temperature. These gradients, in turn, are determined by the profiles of the heating power density and the diffusivities. The diffusivities are strongly affected by the rotation profile, which is also related to the radial gradients of the kinetic quantities as well as the angular momentum input by the heating and the radial flows. Because of this complicated web of internal feedback loops, the long-term evolution of a discharge with high bootstrap fraction needs to be understood.

Experiments have been performed on DIII–D to establish a fully noninductive state without transformer feedback control of the current, under high performance plasma conditions. The discharges are prepared using the transformer, NBI, and ECH to approximate the expected noninductive profiles. Then, to allow the plasma to relax noninductively, either the transformer current is held constant or a novel voltage feedback technique is used to maintain zero voltage at the plasma surface. At $\beta_N \sim 2.0$ and $\beta_p \sim 1.5$ a fully noninductive state with positive dI_p / dt and negative voltage has been maintained for 0.6 s (Fig. 10). The current ramp rate of 30 kA/s agrees with the calculated noninductive current and the estimated resistive relaxation time. The end of the period of current ramp is attributable to a small change in confinement associated with the profile evolution. Working toward

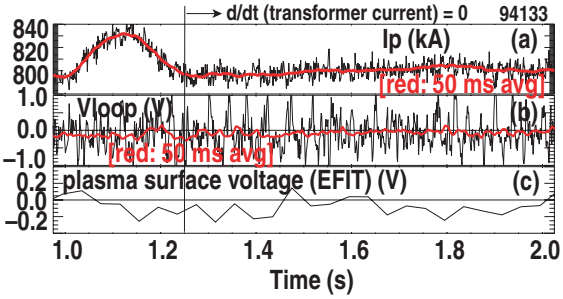

Fig. 10. Fully noninductive ramp of the plasma current. (a) Total plasma current showing dI/dt > 30 kA/s for more than 0.5 s; (b) the voltage measured on a toroidal loop with $\langle V \rangle \lesseqgtr 0$ for the period of the current increase; (c) the voltage at the plasma surface. The vertical line at 1.25 s indicates the beginning of the period of fixed current in the transformer.

higher performance conditions, nearly stationary conditions were maintained for 2.4 s at $\beta_N \sim \beta_p \sim 2.4$. The noninductive state is very sensitive to the inevitable perturbations of small MHD events, particularly as β increases. These studies point out the need to make a systematic study of the behavior of noninductive plasmas operated both near β limits and without transformer feedback.

Summary and conclusions

The DIII-D program is following the AT approach toward steady state operation. By improving the normalized performance (high β_N and H_{89}) through control of the current and rotation profiles, the same real performance can be obtained at reduced plasma current. The reduced current leads to higher bootstrap fraction so that the remaining current can be supported by externally applied current drive without excessive economic penalty. Experiments have demonstrated adequate increases in the normalized performance, but the duration has been limited by evolution of the current profile or by MHD activity. Modeling shows that electron cyclotron current drive using the ECH power under development on DIII–D will support a stationary discharge with potential for steady state, and present experiments on ECCD at the 2 MW power level validate the ECCD efficiency of the modeling. The operation at high β_N introduces the neoclassical tearing mode and the resistive wall mode. The NTM has been shown theoretically and experimentally to be subject to stabilization through application of highly localized ECCD, while the beta limit placed by the RWM can be doubled by improved symmetrization of the confining magnetic fields. The evolution of subtantially stable AT discharges with very high bootstrap fraction is being studied.

Acknowledgment

This is a report of work supported by the U.S. Department of Energy under Contracts DE-AC03-89ER54463, DE-AC05-00OR22725, and DE-AC02-76CH03073, and Grants DE-FG02-89ER54461 and DE-FG03-99ER54541.

References

[1] V.S. Chan et al., Proc. 16th IAEA Fusion Energy Conference, Montreal, 1996 (IAEA, Vienna, 1997), Vol. 1, p. 95.

[2] T.S. Taylor et al., Plasma Physics and Contr. Fusion **39**, 547 (1997).

[3] C.C. Petty et al., Plasma Physics and Contr. Fusion **42(S)**, 75 (2000).

[4] T.C. Luce et al., Nucl. Fusion **41**, 1585 (2001).

[5] M. Murakami et al., 2001 APS DPP presentation, available at http://web.gat.com/pubs-ext/APS01/Murakami_vgs.pdf.

[6] C.C. Petty et al., in *Radio Frequency Power in Plasmas* (Proc. 14th Top. Conf., Oxnard, 2001), (AIP, Melville, New York, 2001), p. 275.

[7] Ronald H. Cohen, Phys. Fluids **30**, 2442 (1987).

[8] R.W. Harvey and M.C. McCoy, in *Proc. IAEA Technical Committee Meeting*, Montreal (IAEA, Vienna, 1993), p. 498.

[9] C.C. Petty et al., in *Radio Frequency Power in Plasmas* (Proc,.13th Top. Conf., Annapolis, 1999), (AIP, Melville, New York, 1999), p. 245.

[10] C.C. Petty et al., Nucl. Fusion **41**, 551 (2001).

[11] T.C. Luce et al., Phys. Rev. Lett. **83**, 4550 (1999).

[12] N.J. Fisch and A.H. Boozer, Phys. Rev. Letters **45**, 720 (1985).

[13] T. Ohkawa, General Atomics Report GA-A13847 (1976).

[14] R. Prater et al., in *Radio Frequency Power in Plasmas* (Proc. 14th Top. Conf., Oxnard, 2001), (AIP, Melville, New York, 2001), p. 302.

[15] R.J. La Haye et al., ‘‘Control of neoclassical tearing modes in DIII–D,” General Atomics Report GA-A23843 (2001); to be published in Physics of Plasmas.

[16] A.M. Garofalo et al., "Sustained rotational stabilization of DIII–D plasma above the no-wall beta limit," General Atomics Report GA-A23864 (2001), to be published in Physics of Plasmas.

[17] Z. Chang et al., Phys. Rev. Lett. **74**, 4663 (1995).

[18] C.C. Hegna and J.D. Callen, Phys. Plasmas **4**, 2940 (1997).

[19] H. Zohm, Phys. Plasmas **4**, 3433 (1997).

[20] G. Gantenbein et al., Phys. Rev. Lett. **85**, 1242 (2000).

[21] R. Prater et al., in *Fusion Energy 2000*, (Proc, 18th Conf,, Sorrento, 2000 (IAEA, Vienna, 2001), paper EX8/1.

[22] A. Isayama et al., Plasma Phys. Contr. Fusion **42**, 137 (2001).

[23] J. Bialek et al., Phys. Plasmas **8**, 2071 (2001).